ASM Handbook, Volume 9: Metallography and Microstructures
G.F. Vander Voort, editor, p134–139
DOI: 10.1361/asmhba0003731

Structures by Precipitation from Solid Solution

Mario Epler, Lehigh University

PRECIPITATION REACTIONS are of great importance in engineering alloys. This general phenomenon occurs in many different alloy systems when one phase (for example γ in steel) transforms into a mixed-phase system (such as $\gamma + \alpha$ in steel) as a result of cooling from high temperatures. The solid-state reaction results in a phase mixture of matrix phase and precipitates that nucleate and coarsen. The matrix may share a similar crystal structure to the parent phase, but has a different composition and often a dissimilar lattice parameter, while the precipitated phase may differ in crystal structure, composition, lattice parameter, and degree of long-range order (Ref 1). The resultant properties of the alloy after precipitation are a direct result of the type, size, shape, and distribution of the precipitated phase.

Phase diagram configurations that give rise to precipitation reactions are shown in Fig. 1. The reaction occurs when the initial phase composition (e.g., α_0, β_0, or I_0) transforms into a two-phase product that includes a new phase, or precipitate. The precipitate phase may differ in crystal structure, composition, and/or degree of long-range order from that of the initial single-phase (parent) phase and the resultant product matrix. The matrix retains the same crystal structure as the initial one-phase parent but with a different equilibrium composition (α, β, or I) and usually a different lattice parameter than the parent phase. This general type of phase change is different from reactions at the invariant points of phase transformation (e.g., a eutectic or peritectic), where any change in temperature or composition results in complete transformation of the parent into a matrix with a different crystal structure. Structures from invariant reactions are discussed in the article "Invariant Transformation Structures" in this Volume.

The length scale of precipitate structures can be quite varied. For example, iron-nickel meteorites that undergo very slow cooling can have macroscopic-scale Widmanstätten structures (see the article "Metallography: An Introduction" in this Volume), while micron-scale precipitate structures occur in moderately to rapidly cooled medium-carbon steel. Precipitation also provides the basis of the strengthening mechanism in age-hardening alloys, where small-scale precipitates (on the order of tens of nanometers) are achieved by carefully controlled heat treatment or thermomechanical processing. Age hardening, which is a controlled precipitation reaction, provides enhanced mechanical properties to commercial alloys. Precipitation reactions are carefully controlled through thermomechanical treatments from supersaturated solid solutions resulting in enhanced strengthening. Precipitation reactions not only provide strengthening, but also wear, creep, and fatigue resistance to alloys.

Age hardening is an important strengthening mechanism, first discovered by Alfred Wilm in the early 1900s from the age hardening of aluminum-copper alloys. It remains an important strengthening mechanism for modern aluminum-copper alloys (as described in more detail in the article "Metallographic Techniques for

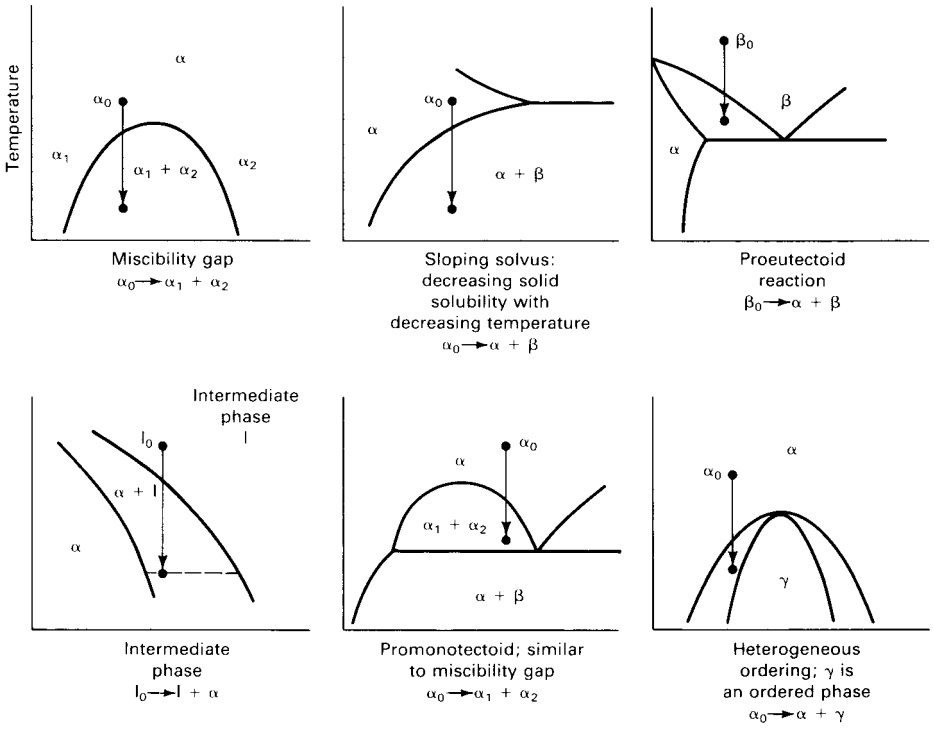

Fig. 1 Equilibrium phase diagrams illustrating various conditions for precipitation of a second phase. In all cases, the matrix of the two-phase product has the same crystal structure as the initial one-phase parent, but with a different equilibrium composition (α, β, or I). Source: Ref 1

Table 1 Surface energies for different types of interfaces

Type of interface	Surface energy
Coherent	$\gamma_{coherent} = \gamma_{chemical} \leq 200$ mJ/m^2
Semicoherent	$\gamma_{semicoherent} = \gamma_{chemical} + \gamma_{structural} \approx 200$ to 500 mJ/m^2
Incoherent	$\gamma_{coherent} \approx 500$ to 1000 mJ/m^2

Aluminum and Its Alloys in this Volume") and many other types of commercial alloys. The typical heat treatment of an age-hardening alloy consists of (Ref 2):

1. Solution treating (solutionizing) that results in a homogenous supersaturated solid solution
2. Quenching to a temperature in the two-phase region (generally room temperature) to retain a supersaturated solid solution
3. Aging at an elevated temperature to control the precipitation of the second phase from the solid solution

In addition, thermomechanical processing, which involves cold working the as-quenched alloy before aging, is sometimes used. The deformation can affect the subsequent precipitation reaction kinetics and modify the resultant properties through dislocation generation and the influence of strain hardening. Quenching directly to the aging temperature also can influence the kinetics and reaction path in the decomposition of the supersaturated parent phase.

Nucleation and Growth

Nucleation, growth, and coarsening are important in determining the resultant microstructure of the precipitates and associated mechanical properties. During nucleation, not only is the type of precipitate that forms important, but also the distribution of the precipitates. Distribution of precipitates influences mechanical strength by affecting dislocation motion.

Nucleation can occur either homogenously (uniformly and nonpreferentially) or heterogeneously (preferentially) at specific sites such as grain boundaries or dislocations. Most precipitates involve or require the presence of preferential sites for heterogeneous nucleation, but Guinier-Preston (GP) zones and other fully coherent precipitates (such as Ni_3Al in nickel-base superalloys) nucleate homogeneously. Coherent precipitation occurs when continuity is maintained between the crystal lattice of the precipitate and the lattice of the matrix.

Typical heterogeneous nucleation sites include crystal defects such as grain boundaries, grain corners, vacancies, or dislocations. Heterogeneous nucleation occurs because the elimination of defects and high-energy surfaces (by the nucleation of a new phase) acts to reduce the overall free energy of the system. The rate of heterogeneous nucleation thus is influenced by the density of these irregularities. The free-energy relationships associated with homogenous and heterogeneous nucleation can be described as (Ref 2):

$$\Delta G_{hom} = -V(\Delta G_v - \Delta G_s) + A\gamma$$

$$\Delta G_{het} = -V(\Delta G_v - \Delta G_s) + A\gamma - \Delta G_d$$

where:

ΔG_{hom} is the total free-energy change for homogeneous nucleation.

ΔG_{het} is the total free-energy change for heterogeneous nucleation.

V is the volume of transformed phase.

ΔG_v is the volume free energy of transformed phase.

ΔG_s is the volume misfit strain energy of transformed phase.

$A\gamma$ is the surface area and surface energy term of transformed phase, assuming isotropic.

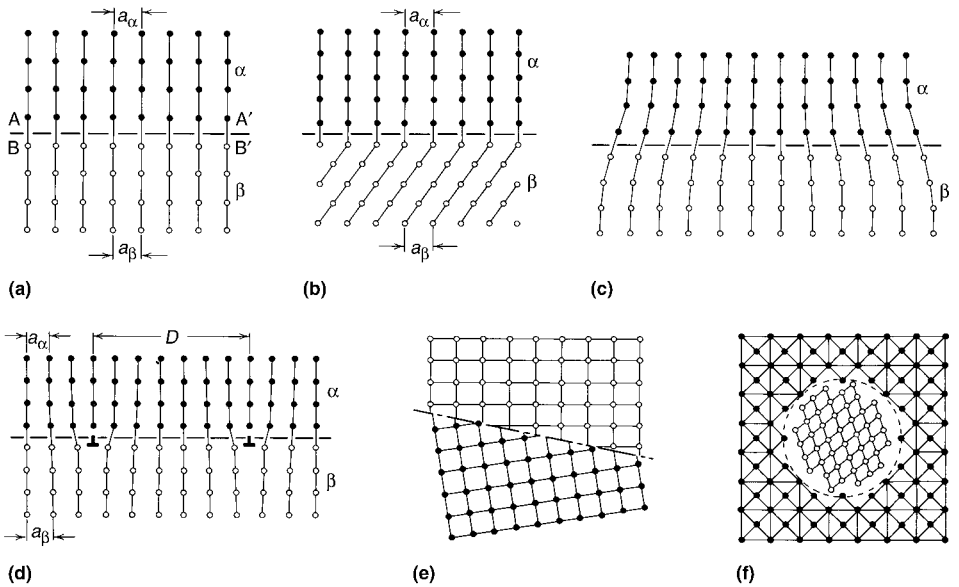

Fig. 2 Different types of interfaces. (a) and (b) Fully coherent. (c) and (d) Semicoherent showing lattice strain and the presence of dislocations. (e) and (f) Incoherent. Source: Ref 1

Table 2 Crystallographic relations between precipitate and parent phases in selected alloy systems

Alloy system	Parent phase and lattice(a)	Precipitate phase and lattice(a)	Crystallographic relations (precipitate phase described first)
Ag-Al	Al solid solution; fcc	γ (Ag_2Al); hcp	(0001) ∥ (111), [11$\bar{2}$0] ∥ [1$\bar{1}$0]
	Al solid solution; fcc	γ′ (transitional); hcp	(0001) ∥ (111), [1120] ∥ [110]
Ag-Cu	Ag solid solution; fcc	Cu solid solution; fcc	Plates ∥ {100}; all directions ∥
	Cu solid solution; fcc	Ag solid solution; fcc	Plates ∥ {111} or {100}; all directions ∥
Ag-Zn	β (βAgZn); bcc	Ag solid solution; fcc	(111) ∥ (110), [110] ∥ [111]
	β (βAgZn); bcc	γ (γAg_5Zn_8); bcc	(100) ∥ (100), [010] ∥ [010]
Al-Cu	Al solid solution; fcc	θ ($CuAl_2$); bct	Plates ∥ (100); (100) ∥ (100), [011] ∥ [120]
	Al solid solution; fcc	θ′ (transitional); tet	(001) ∥ (100), [010] ∥ [011]
Al-Mg	Al solid solution; fcc	β (β-Al_3Mg_2); fcc	Plates first ∥ {110}; later probably ∥ {120}
Al-Mg-Si	Al solid solution; fcc	Mg_2Si; fcc	Plates ∥ {100}
Al-Zn	Al solid solution; fcc	Nearly pure Zn; hcp	Plates ∥ {111}; (0001) ∥ {111}, [11$\bar{2}$0] ∥ ⟨110⟩
Au-Cu (b)	Au-Cu solid solution; fcc	α_1' (AuCu I); ord fct	(100) ∥ (100), [010] ∥ [010]
Be-Cu	Cu solid solution; fcc	γ_2 (γBeCu); ord bcc	G-P zones ∥ {100}; later γ_2 with [100] ∥ [100], [010] ∥ [011]
0.4C-Fe	Austenite (γFe); fcc	Ferrite (αFe) (proeutectoid); bcc	(110) ∥ (111), [1$\bar{1}$1] ∥ [1$\bar{1}$0]
0.8C-Fe	Austenite (γFe); fcc	Ferrite in pearlite; bcc	(011) ∥ (001), [$\bar{1}$00] ∥ [100], [0$\bar{1}$1] ∥ [010]
	Austenite (γFe); fcc	Ferrite in upper bainite; bcc	(110) ∥ (111), [1$\bar{1}$0] ∥ [2$\bar{1}$1]
		Ferrite in lower bainite; bcc	(110) ∥ (111), [1$\bar{1}$1] ∥ [110]
1.3C-Fe	Austenite (γFe); fcc	Cementite (Fe_3C); ortho	Plates not ∥ (111); (001) Fe_3C ∥ to plane of plate
Co-Cu	Cu solid solution; fcc	αCo solid solution; fcc	Plates ∥ {100}; lattice orientation same as parent matrix
Co-Pt(b)	Pt-Co solid solution; fcc	α″ (CoPt); ord fct	Plates ∥ {100}; all directions ∥
Cu-Fe	Cu solid solution; fcc	γFe (transitional); fcc	Cubes {100}; lattice orientation same as parent matrix
		αFe; bcc	Plates ∥ {111}; lattice orientation random
Cu-Si	Cu solid solution; fcc	β (ζ Cu-Si); hcp	Plates ∥ {111}; (0001) ∥ (111), [1120] ∥ [110]
Cu-Sn	β phase; bcc	Cu solid solution; fcc	(111) ∥ (110), [1$\bar{1}$0] ∥ [1$\bar{1}$1]
Cu-Zn	β (CuZn); bcc	Cu solid solution; fcc	(111) ∥ (110), [110] ∥ [111]; variable habit; plates or needles ∥ [556]
	β (CuZn); bcc	γ (γCu_5Zn_8); ord bcc	(100) ∥ (100), [010] ∥ [010]
	ε (εCu-Zn); hcp	Zn solid solution; hcp	(1014) ∥ (1014), [1120] ∥ [11$\bar{2}$0]
Fe-N	Ferrite (αFe); bcc	γ_1 (Fe_4N); fcc	(112) ∥ (210)
Fe-P	Ferrite (αFe); bcc	δ (Fe_3P); bct	Plates ∥ (21,1,4)
Pb-Sb	Pb solid solution; fcc	Sb solid solution; rhom	(001) ∥ (111), [100] ∥ [1$\bar{1}$0]

(a) bcc, body-centered cubic; bct, body-centered tetragonal; fcc, face-centered cubic; hcp, hexagonal close-packed; ord bcc, ordered body-centered cubic; ord fct, ordered face-centered tetragonal; ortho, orthorhombic; rhom, rhombohedral; tet, tetragonal. (b) Ordering transformation. Source: Ref 1

ΔG_d is the free energy resulting from destruction of defect.

Additionally, typical values for surface energy are summarized in Table 1, and various interfaces are shown in Fig. 2. Faceted interfaces often are coherent, while nonfaceted interfaces are semicoherent or incoherent. As long as there is a sufficient density of heterogeneous nucleation sites, homogeneous nucleation will not be favored. Table 2 lists some selected precipitation reactions in different alloys and the crystallographic relations between the parent and precipitated phases.

A coherent interface (Fig. 2a and b) is characterized by atomic matching at the boundary and a continuity of lattice planes, although a small mismatch between the crystal lattices can lead to coherency strains (Fig. 2c). Coherent interfaces have a relatively low interfacial energy that typically ranges from 50 to 200 ergs/cm^2 (0.05 to 0.2 J/m^2).

An incoherent interface (Fig. 2e and f) is an interphase boundary that results when the matrix and precipitate have very different crystal structures and little or no atomic matching can occur across the interface. The boundary is essentially a high-angle grain boundary characterized by a relatively high interfacial surface energy (~500 to 1000 ergs/cm^2, or 0.5 to 1.0 J/m^2).

Semicoherent interfaces (Fig. 2d) represent an intermediate case in which it becomes energetically favorable to partially relax the coherency strains, which would develop if perfect matching occurred across the boundary by introducing an array of misfit dislocations. These interfaces, which are characterized by regions of good fit punctuated by dislocations that accommodate some of the disregistry, have interfacial surface energies from 200 to 500 ergs/cm^2 (0.2 to 0.5 J/m^2).

Dislocations act as nucleation sites only for semicoherent precipitates (Ref 2). Figure 3 (Ref 3) shows precipitates forming at dislocations. The formation of semicoherent precipitates usually results in the generation of dislocations as a result of the lattice mismatch. The generation of a dislocation maintains coherency by relaxing the strains that develop because of the difference in the lattice parameter at the interface. Vacancies play several roles in the nucleation of precipitates. Vacancies allow for appreciable diffusion at temperatures where diffusion is not expected. They also act to relieve local strain allowing for the nucleation coherent precipitates. Vacancy concentration is dependent on temperature, so it is essential for high quenching rates to not only maintain a supersaturated solid solution but to retain significant numbers of vacancies.

Accompanying the precipitation sequence is the change in the chemistry of the matrix phase. As more and larger precipitates form, the solute is depleted in the matrix. Areas where no precipitates form are termed precipitate-free zones (PFZs) or denuded areas. These typically occur around grain boundaries or second-phase particles where the solute is trapped (Fig. 4) or re-

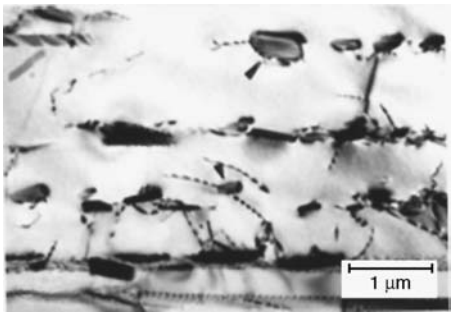

Fig. 3 Transmission electron microscopy bright field micrograph showing Ti_5Si_3 precipitates at dislocations in a $Ti_{52}Al_{48}$-3Si2Cr alloy. Source: Ref 6

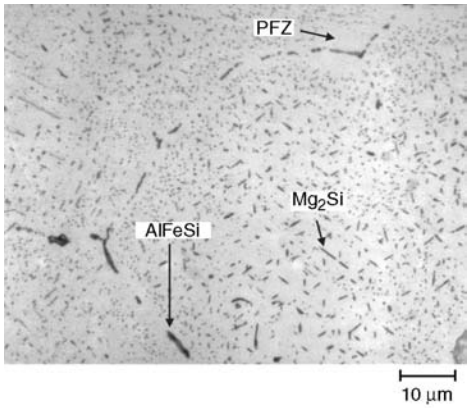

Fig. 4 Micrograph of cast and homogenized 6061 aluminum alloy, showing the precipitate-free zone (PFZ) (lack of Mg_2Si precipitates) at grain boundary. The PFZ was created by the lack of silicon, which is wrapped up in the AlFeSi precipitates at the grain boundary. Source: Ref 4

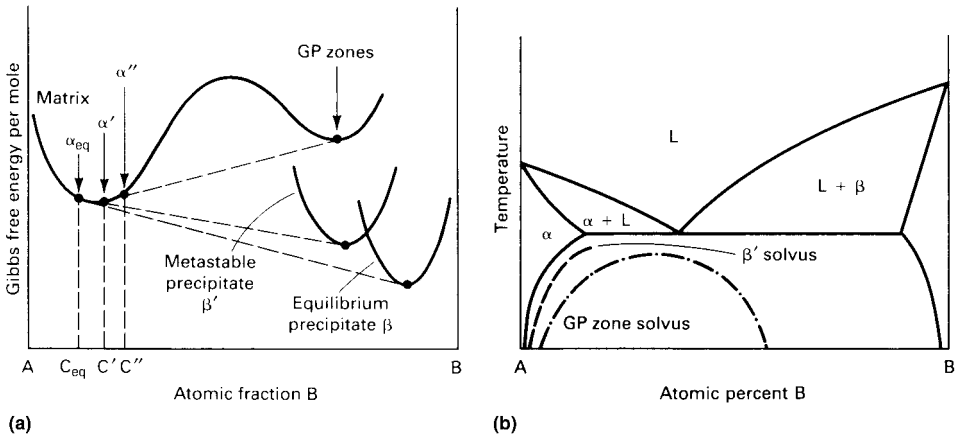

Fig. 5 Gibbs free-energy composition diagram (a) and locus of solvus curves (b) of metastable and stable equilibrium phases in a precipitation sequence. (a) The points of common tangency show the relationship between compositions of the matrix phase (C″, C′, and C_{eq}) and the various forms of precipitate phases at a given temperature. From this common tangent construction, it can be see that for the small Guinier-Preston zones, there is a higher solubility in the matrix. (b) Hypothetical phase diagram showing the locus of metastable and stable solvus curves. Source: Ref 1

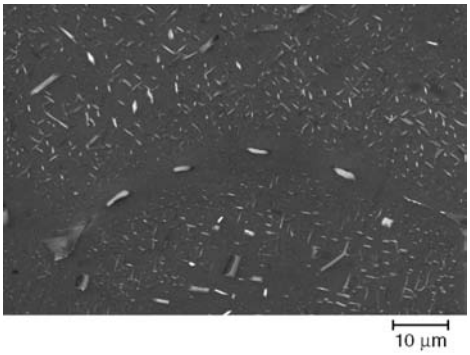

Fig. 6 Scanning electron micrograph of continuous precipitation in 6061 aluminum alloy, where the smaller precipitates are Mg_2Si, and the larger particles are AlFeSi intermetallics at the grain boundary. Note the precipitate-free zone near the AlFeSi intermetallics. Source: Ref 5

Fig. 7 Transmission electron micrograph showing a region of discontinuous (left) and continuous (right) precipitation in a specimen of AZ91 aged at 200 °C (390 °F) for 4 h. Source: Ref 6

gions where there are insufficient vacancies to nucleate precipitates.

Coarsening of the particles occurs because the microstructure of a two-phase alloy is not stable unless the interfacial energy is at a minimum. A lower density of larger particles has less total interfacial energy than a high density of small particles, which provides the driving force for particle coarsening. Particle coarsening is driven by diffusion of solute atoms; thus, the rate of coarsening increases with temperature. In some cases, coarsening rates are determined by interface control.

Ostwald ripening is the mechanism where the smaller precipitates dissolve and the solute is redistributed to the larger stable precipitates. The higher solubility of the smaller particles in the matrix is termed the capillary effect and can be seen on a free-energy diagram (Fig. 5a). Smaller particles have a higher free energy due to increased pressure because of high surface curvature. The point of common tangent (Fig. 5a) therefore occurs at a higher solute concentration.

Growth of precipitates occurs by either movement of the incoherent interfaces or a ledge mechanism where coherency is maintained while thickening due to diffusion (Ref 1, 2). Reversion occurs when an alloy containing GP zones or intermediate semicoherent phase is heated above their respective solvus temperatures and they redissolve into the matrix.

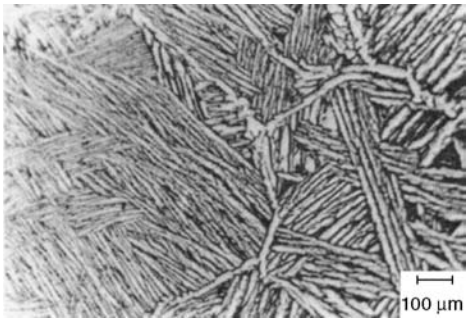

Fig. 8 Widmanstätten structure in Ti-6Al-4V alloy cooled at 3.40 °C/s (6.12 °F/s). Source: Ref 7

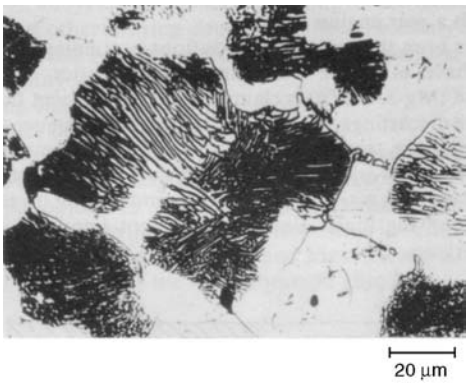

Fig. 9 Discontinuous precipitation of β phase ($Mg_{17}Al_{12}$) in cast AZ80 zirconium-free magnesium casting alloy. Source: Ref 9

Precipitation Modes

General or continuous precipitation refers to the uniform appearance of second-phase particles throughout the grains of the matrix. General precipitation does not imply homogeneous nucleation, rather, the nonlocalized precipitation of the second phase. Discontinuous precipitation can occur at regions such as grain boundaries, or cellular precipitation where precipitation begins at grain boundary allotriomorphs but does not continue through the entire grain. Figures 4 and 6 show general precipitation in aluminum alloys. Figure 7 (Ref 6) shows a contrast between discontinuous and continuous precipitation in AZ91, a Mg-Al-Zn alloy.

Widmanstätten Structures. The continuous precipitation of plate or lathlike structures is referred to as Widmanstätten morphology. This distinctive plate or lathlike morphology is characterized by the presence of both high- and low-angle boundaries. Widmanstätten morphologies form in many alloy systems. This is illustrated in Fig. 8 (Ref 7), a Ti-6Al-4V alloy. As evident by the microstructure, there are specific orientation relations between the precipitate habit plane and matrix (Ref 1, 2). The long broad faces of the precipitates are the coherent, low-energy interfaces (Ref 1, 2). During growth, small ledges form on these faces, allowing for diffusional thickening while maintaining coherency. Typically, this morphology forms during low cooling rates, but the Widmanstätten morphology can occur if a sufficient driving force for growth is provided by either a fast cooling rate or large undercooling (Ref 8). As Ref 8 describes,

> The development of the side plate morphology normally starts from a grain

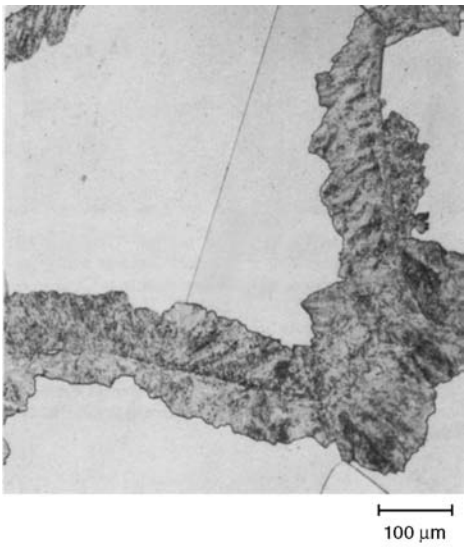

Fig. 11 Cellular colonies growing out from grain boundaries in Au-30Ni alloy aged 50 min at 425 °C (795 °F). Etchant: 50 mL 5% ammonium persulfate and 50 mL 5% potassium cyanide. 100×. Courtesy of R.D. Buchheit. Source: Ref 1

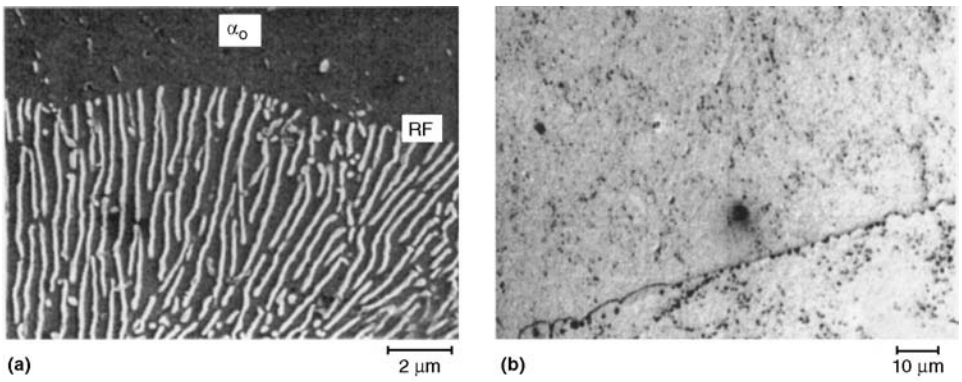

Fig. 10 Discontinuous precipitation (DP). (a) Scanning electron micrograph of lamellar structure within a DP cell Mg-10Al (wt%) annealed at 500 K for 40 min. RF, reaction front; α_0, supersaturated solid solution. (b) Light optical micrograph of early stage of the DP reaction in Mg-10Al (wt%) annealed at 500 K for 20 min. The bowing out of the grain boundary between two allotriomorphs is clearly seen. Source: Ref 10

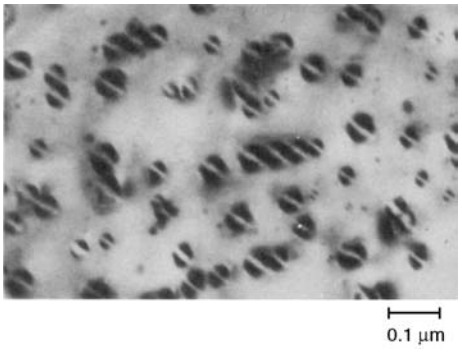

Fig. 12 Coherent transition precipitates revealed by strain contrast (dark-field) in transmission electron microscopy. The specimen is a Cu-3.1Co alloy aged 24 h at 650 °C (1200 °F). The precipitate is a metastable face-centered cubic (fcc) phase of virtually pure cobalt in the fcc matrix. The particles are essentially spherical, and the "lobe" contrast is characteristic of an embedded "misfitting sphere." This strain contrast reveals the particles indirectly through their coherency strain fields. Original magnification 70,000×. Courtesy of V.A. Phillips

boundary allotriomorph (as in the case of steels) and growth occurs into the grain. As cooling rates increase, the diffusion of atoms to the high-angle boundaries (where no special orientation exists between austenite and ferrite) is slow, but if diffusion distances are minimized by phase morphology and growth occurs in preferred crystallographic directions, growth rates can be increased.

Cellular or Discontinuous Precipitation. Grain-boundary precipitation may result in cellular or discontinuous precipitation (DP). Figures 9 (Ref 9) and 10 show examples of the alternating lamellar structure that is common to many cellular precipitation transformations. During discontinuous precipitation, the second phase nucleates at the grain boundary, which then moves with the advancing precipitation reaction. It typically starts at a high-angle incoherent boundary, which is the most likely point to support the process of heterogeneous nucleation and boundary migration. Misfit or atomic mismatch strain are factors, although neither misfit nor atomic mismatch strain appear to be necessary conditions in several instances (e.g., Al-Li, Ni-Al, Ni-Ti, Al-Ag, and Cu-Co) (Ref 11, 12). The general conditions and criteria of DP are not completely understood due to the complex interrelationships among boundary structure, energy, mobility, and diffusivity.

Following nucleation, the grain boundary moves with the advancing precipitation reaction. This is illustrated in Fig. 10(b), where the grain boundary is seen bowing out at the beginning of the reaction (Ref 9). Morphologically, it resembles eutectoid decomposition (see the article "Invariant Transformation Structures" in this Volume). Discontinuous precipitation results in reaction products that are often lamellar, fibrous, or rodlike, but rarely globular (Ref 11). Discontinuous precipitation is also often referred to as a cellular, grain-boundary, recrystallization, or autocatalytic reaction (Ref 13).

Lamellar spacing of the precipitates is dependent on aging temperature, with wider spacing occurring higher temperatures. Free energy is limited for creating of interfaces due to the lower driving force (at higher temperature). It is termed discontinuous because the matrix composition changes discontinuously as the cell advances. Cellular precipitation is also observed in Fig. 11, clearly showing the relationship between the cells and the grain boundaries.

Precipitation Sequences

In many precipitation systems and in virtually all effective commercial age-hardening alloys, the supersaturated matrix transforms along a multistage reaction path, producing one or more metastable transition precipitates before the appearance of the equilibrium phase. The approach to equilibrium is controlled by the activation (nucleation) barriers separating the initial state from the states of lower free energy. The transition precipitates are often crystallographically similar to the matrix, allowing the formation of a low-energy coherent interface during the nucleation process.

Often the precipitation sequence begins with the nucleation of small, fully coherent phases known as Guinier and Preston zones (discovered

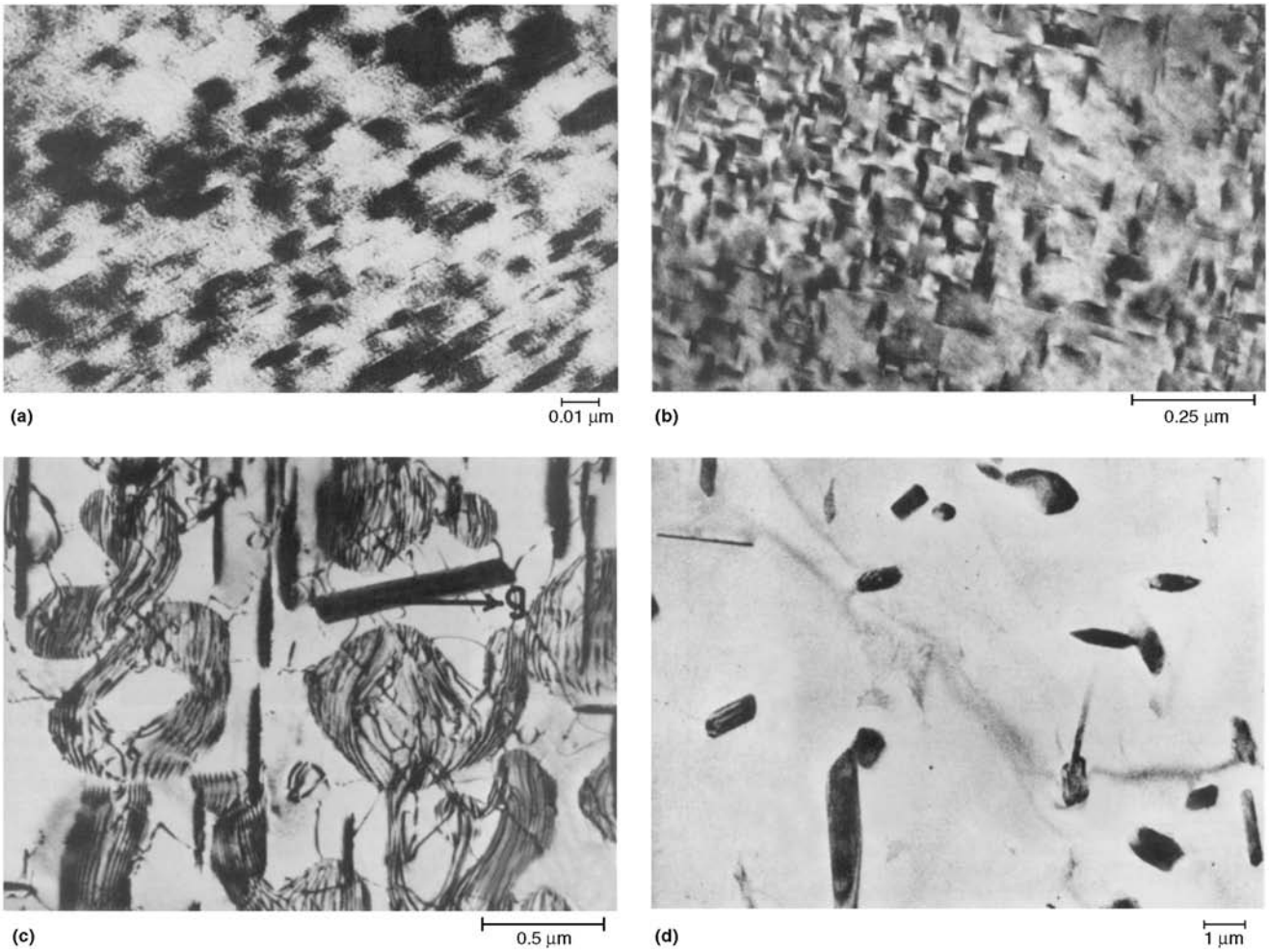

Fig. 13 Transmission electron micrographs of precipitation sequence in aluminum-copper alloys. (a) Guinier-Preston zones at 720,000×. (b) θ″ at 63,000×. (c) θ′ at 18,000×. (d) θ at 8000×. Source: Ref 2

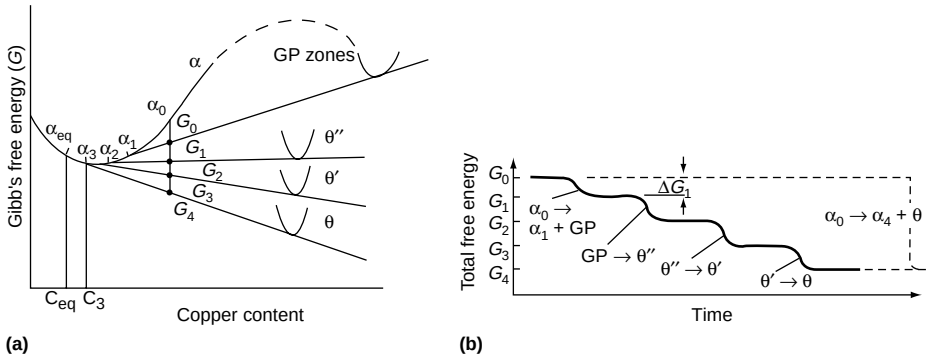

Fig. 14 Free-energy plots of precipitation sequence in aluminum-copper alloys. (a) Free-energy curve with common-tangent points for phase compositions in the matrix. (b) Step reductions in the free energy as the transformation proceeds. C_{eq} and C_3, copper content of α_{eq} and α_3 phases; ΔG_1, activation energy for $\alpha_0 \rightarrow \alpha_1 + GP$. GP, Guinier-Preston. Source: Ref 4

independently by Guinier and Preston from x-ray diffraction studies). Guinier-Preston (GP) zones are solute-rich clusters resulting from phase separation or precipitation within a metastable miscibility gap in the alloy system. They may form by homogeneous nucleation and grow at small undercoolings or by spinodal decomposition at large undercoolings or supersaturations (see the article "Spinodal Transformation Structures" in this Volume).

The GP zones are the first to nucleate because of their small size and coherency with the matrix. The interfacial energy term is extremely low, providing a low barrier to nucleation, although the driving force for nucleation may not be as high as for the final phase to form. The GP zones typically take the shape of small spherical particles or disk-shaped particles (Fig. 12) that are about two atomic layers thick and several nanometers in diameter aligned perpendicular to the elastically soft direction in the matrix material crystal structure (Ref 2). The GP precipitates generally grow into more stable transition phases and eventually an equilibrium phase.

The phases that nucleate and grow from the GP zones are termed "transition phases." They have an intermediate crystal structure between the matrix and equilibrium phase. This minimizes the strain contribution to energy between the precipitate and the matrix, making it more favorable in the nucleation sequence than the equilibrium phases, which is incompatible with the matrix and has high interfacial energy. A typical reaction sequence for aluminum-copper systems is shown in Fig. 13 can be written as:

$$\alpha_0 \rightarrow \alpha_1 + GPZ \rightarrow \alpha_2 + \theta'' \rightarrow \alpha_3 + \theta' \rightarrow \alpha_{eq} + \theta$$

where θ' and θ'' are transition precipitates and θ is the equilibrium precipitate. Composition of each phase and the matrix can be determined by the common tangent method applied to Fig. 14(a). As each new precipitate forms, the matrix (α) becomes more and more depleted in copper. The GP zones and θ'' precipitates are resolved in transmission electron microscopy (TEM) because of the lattice coherency strains. Each step results in the previously precipitated phase being replaced with the new, more stable phase. Figure 14(b) outlines the step reductions in total free energy for reactions in the precipitation sequence. The size of the step reduction is the activation energy for a transformation.

To maximize strengthening, aging is typically carried out to the precipitation between θ'' and θ', because spacing and lattice strain are ideal to hinder dislocation motion. Reactions carried out beyond maximum strengthening are termed overaged, because the beneficial effects of precipitation strengthening are lost as the precipitates grow larger in size and spacing.

ACKNOWLEDGMENT

Portions of this article are adapted from the article by W.A. Soffa, "Structures Resulting from Precipitation from Solid Solution," in *Metallography and Microstructures*, Volume 9, *ASM Handbook*, 1985, pages 646–650 (Ref 1).

REFERENCES

1. W.A. Soffa, Structures Resulting from Precipitation from Solid Solution, *Metallography and Microstructures*, Vol 9, *ASM Handbook*, ASM International, 1985, p 646–650
2. D.A. Porter and K.E. Easterling, *Phase Transformations in Metals and Alloys*, 2nd ed., Chapman and Hall, 1996, p 514
3. F.-S. Sun and F.H. Sam Froes, Precipitation of Ti_5Si_3 Phase in TiAl Alloys, *Mater. Sci. Eng. A*, Vol 328 (No. 1–2), 2002, p 113–121
4. W.H. Van Geertruyden, W.Z. Misiolek, G.G. Lea, and R.M. Kelly, Thermal Cycle Simulation of 6xxx Aluminum Alloy Extrusion, *Proc. Seventh International Extrusion Technology Seminar* (Chicago, IL) Aluminum Extruders Council, 2000
5. S.R. Claves, D.L. Elias, and W.Z. Misiolek, Analysis of the Intermetallic Phase Transformation Occurring During Homogenization of 6xxx Aluminum Alloys, *Proc. International Conference of Aluminium Alloys 8*, Trans Tech Publications, Cambridge, U.K., 2002
6. S. Celotto and T.J. Bastow, Study of Precipitation in Aged Binary Mg-Al and Ternary Mg-Al-Zn Alloys Using ^{72}AlNMR Spectroscopy, *Acta Mater.*, Vol 49, 2001, p 41–51
7. F.J. Gil, M.P. Ginebra, J.M. Manero, and J.A. Planell, Formation of Widmanstätten Structure: Effects of Grain Size and Cooling Rate on the Widmanstätten Morphologies and on the Mechanical Properties in Ti6Al4V Alloy, *J. Alloy. Compd.*, Vol 329 (No. 1–2), 2001, p 142–152
8. A. Tomer, *Structure of Metals through Optical Microscopy*, ASM International, 1991, p 113–114
9. I.J. Polmear, *Light Alloys—Metallurgy of the Light Metals*, 3rd ed., Arnold, 1995
10. D. Bradai, P. Zieba, E. Bischoff, and W. Gust, Correlation between Grain Boundary Misorientation and the Discontinuous Precipitation Reaction in Mg-10 wt.% Al Alloy, *Mater. Chem. Phys.*, Vol 78 (No. 1), 2003, p 222–226
11. I. Manna, S.K. Pabi, and W Gust, Discontinuous Reactions in Solids, *Int. Mater. Rev.*, Vol 46 (No. 2), 2001, p 53–91
12. M. Shaarbaf and R.A. Fournelle, *Mater. Sci. Eng. A*, Vol 102, 1988, p 271–279
13. D.B. William and E.P Butler, Grain Boundary Discontinuous Precipitation Reactions, *Int. Met. Rev.*, Vol 26 (No. 3), 1981, p 153–183